Novel Parametric PET Image Quantification using Texture and Shape Analysis

A. Rahmim, J. Coughlin, M. Gonzalez, C. J. Endres, Y. Zhou, D. F. Wong, R. L. Wahl, V. Sossi, M. G. Pomper

Abstract– **Kinetic parameter estimation at the individual voxel level has the powerful ability to represent both spatial distributions and quantitative physiological parameters of interest. In practice, parametric images are commonly quantified by computing mean values for specified ROIs. Nonetheless, the mean operator vastly oversimplifies the available spatial uptake information. It may be hypothesized that a given tracer will exhibit increasingly differential or heterogeneous uptake due to disease: subsequently, we have implemented and explored a comprehensive texture and shape analysis framework wherein extensive information is generated from parametric PET images, through: (1) 3D moment invariants analysis, (2) intensity histogram analysis, (3) gray-level spatial-dependence (GLSD) analysis, and (4) neighborhood gray tone difference (NGTD) analysis. In the present work, we applied this approach to imaging of 11C-DPA-713, a novel PET ligand with high binding to the translocator protein (TSPO), a marker of neuroinflammation. In particular, for tracers such as DPA with relatively wide-spread uptake, where a reliable reference tissue does not exist, quantification of heterogeneity may provide additional valuable information. Our center has been the first to perform DPA PET studies in humans, and is gathering a large collection of PET studies; e.g. subjects with systemic lupus erythematosus (SLE), traumatic brain injury (TBI; former NFL players), along with young and elderly controls. Our preliminary analysis has revealed that, compared to conventional mean ROI analysis, a number of metrics in the proposed framework yield enhanced discrimination (as measured using AUC) between patients vs. controls in a range of ROIs, in TBI as well as SLE vs. controls, consistent with increased heterogeneity of uptake with disease, though in the case of SLE this can be, at least partly, attributed to changes in ROI shapes. Overall, the proposed framework has the potential to bring about a new quantification paradigm in parametric imaging.**

I. INTRODUCTION

Dynamic PET imaging provides the ability to extract important physiological and biochemical parameters of interest [1]. Kinetic parameters are commonly estimated from time-activity curves from each region-of-interest (ROI) [2]. This approach can also be applied at the individual voxel level, leading to parametric images: these images are in practice quantitatively summarized by computing mean values for specified ROIs. An observation serving as the premise of the present work is that the mean operator vastly oversimplifies the available spatial uptake information. Here we have implemented a comprehensive texture and shape analysis framework wherein more extensive information is generated from parametric PET images, potentially leading to enhanced ability to discriminate among different populations and tasks. This approach has an analogue in studies of tumor heterogeneity (as induced by regional variations in proliferation, cell death, vascular structure, etc.)[3] whereby a number of recent FDG PET studies indicated enhanced prediction of patient outcome [4] and therapeutic response [5, 6] based upon such quantification. Our proposed framework promises to aid studies involving radiotracers hypothesized to exhibit intra-regional heterogeneity and/or shape changes due to disease. In particular, for radiotracers with widely distributed uptake where a reliable reference tissue may not exist, quantification of heterogeneity may provide additional valuable information.

II. METHODS

Our comprehensive framework consists of four general analytic schemes, which we elaborate next.

A. Analysis using 3D moment invariants (3D-MIs)

We have used 3D-MIs to characterize ROI spatial distributions. MIs are mathematical spatial descriptors designed to be invariant to scaling, translation and rotation, with extensive use in a number of areas including pattern recognition [7], and with recent in an fMRI study to assess spatial characteristics of voxel-based statistics [8]. We have recently demonstrated (i) significant shape differences in striatal ROI PET uptake between healthy controls and patients with Parkinson's disease (PD) imaged using pre-synaptic and post-synaptic radiotracers [9], and (ii) significant correlation of PD disease severity with shape (and change in shape upon administration of stimulant) [9, 10]. Here we apply second-order J_1, J_2, J_3, Q and third-order B_3 3D-MIs [8, 11, 12] to quantify ROI PET uptake.[1] We also apply these to ROI definitions wherein values within the ROI are set to 1 (and 0 otherwise) to assess anatomic shape differences (e.g. due to atrophy) between subject populations, which could provide further quantitative information and study confounding impacts of the partial volume effect (PVE).

B. Analysis of intensity histograms

One approach to assess within-ROI heterogeneity is to analyze first-order statistics via the intensity histogram;

Manuscript received November 4, 2012.

A. Rahmim, J. Coughlin, C. J. Endres, Y. Zhou, D. F. Wong, R. L. Wahl and M. G. Pomper are with the Department of Radiology, Johns Hopkins University, Baltimore, MD, USA 21287 (telephone: 410-502-8579, e-mail: arahmim1@jhmi.edu).

M. Gonzalez and V. Sossi are with the Department of Physics & Astronomy, University of British Columbia, Vancouver, BC, Canada V6T 1Z1.

[1] In fact, $J_2 = \frac{1}{2}\left(J_1^2 - Q\right)$, and as such, typically Q is not considered separately.

standard deviation (*std*), skewness and kurtosis of the distribution are generated (in addition to %std relative to mean uptake). One may also perform cumulative histogram analysis leading to the intensity-volume histogram [6], a decreasing function of intensity *I* that we represent as:

$$V^{ROI}(I) = \frac{1}{N}\sum_{i \in ROI} \delta_{f_i \geq I} \quad (1)$$

which quantifies the fraction of all voxels *i* (relative to the entire ROI of size *N*) that have values f_i at least as small as *I*. One can then define I_x such that $V^{ROI}(I_x) = x\%$. We also define V_x as the fraction of volume containing at least *x%* of the maximum intensity in the ROI. One can then similarly define such differential metrics as $I_{10-90} = I_{10} - I_{90}$ and $V_{50-90} = V_{50} - V_{90}$ to quantify heterogeneity in the overall histogram. Nonetheless, a shortcoming of histogram analysis is that it is global and does not quantify local variations in uptake.

C. Gray-level spatial-dependence (GLSD) analysis

The GLSD matrix, more commonly known as the co-occurrence matrix [13], estimates the second order joint conditional probability density function that two voxels separated along a certain direction by a certain distance have respective (discretized) gray levels *i* and *j*. Based on the co-occurrence matrix, a number of so-called Haralick texture measures may be computed; we considered twelve measures [13, 14]: (1) energy, (2) entropy, (3) correlation, (4) contrast (also known as inertia [15, 16]), (5) variance, (6) sum mean, (7) agreement [17] (also known as Cohen's [18] κ-statistic), (8) cluster shade, (9) cluster tendency (or prominence), (10) homogeneity, (11) max probability, and (12) inverse variance. A comparable, computationally more feasible formulation to the co-occurrence matrix utilizes gray-level difference statistics (GLDS) [19]. Here we computed the co-occurrence matrix using a combination of 13 directions (3D neighborhood) and four distances of 1, 2, 3 and 4 voxels.

D. Neighborhood gray tone difference (NGTD) analysis

The abovementioned formulation can be relatively complex due to having a number of free variables (direction, distance) and the two-dimensionality of the co-occurrence matrix. An alternative formulation [20] is to generate the NGTD vector:

$$s(i) = \sum_{i \in N_i} \left| i - \overline{A}_i \right| \quad (2)$$

where N_i is the set of all voxels with gray level *i*, and $\overline{A}_i$ is the average gray-tone over a neighborhood (26 voxels in 3D in this work) centered around the voxel. We observed that *s(i)* needed to be normalized to ROI size to avoid confounding due to varying ROI sizes among patients. Next, five textural features, corresponding to visual properties of texture [20], were computed: (1) coarseness, (2) contrast, (3) busyness, (4) complexity, and (5) strength.

III. APPLICATION TO PET STUDIES

We plan to apply the abovementioned framework to a wide range of radiotracers, to assess differential or heterogeneous uptake with (and within) disease. A compound we have studied is ^{11}C-DPA-713, a novel PET ligand with high binding to the translocator protein (TSPO), a marker of neuroinflammation. We performed the initial ^{11}C-DPA-713 PET studies in humans [21], and are gathering a large collection of such studies on subjects with a wide variety of neuroinflammatory illnesses, along with young and elderly controls. We have preliminarily evaluated the following subject sets: 5 with systemic lupus erythematosus (SLE) vs. 10 controls, and 5 with traumatic brain injury (TBI) vs. 3 controls.

A. Figures-of-merit (FOM)

It is useful to pose our quantification problem as a discrimination task: a simple FOM for the discriminatory value of a given metric is the distance between the two subject classes (with respective means m_1,m_2 and standard deviations σ_1,σ_2), represented as the signal-to-noise ratio (SNR):

$$SNR = \frac{m_1 - m_2}{\sqrt{\frac{1}{2}\sigma_1^2 + \frac{1}{2}\sigma_2^2}} \quad (3)$$

Moreover, under assumption of normal distribution, the area under the ROC curve (AUC) can be extracted from the *SNR* according to [22]:

$$AUC = \frac{1}{2} + \frac{1}{2} erf\left(\frac{SNR}{2}\right) \quad (4)$$

where *erf()* is the error function defined by:

$$erf(z) = \frac{2}{\sqrt{\pi}} \int_0^z dy\ e^{-y^2} \quad (5)$$

B. Results and discussion

Compared to standard metrics of mean distribution volume (DV) and DV ratio (DVR; where caudate was used as the reference tissue), a number of metrics in the proposed framework yielded considerably enhanced discrimination (as measured using AUC) between patients vs. controls in a range of ROIs. The results are depicted for TBI vs. controls in **Table 1** and for SLE vs. controls in **Table II**, and are consistent with increased heterogeneity of uptake with disease.

Table I: AUC values (TBI vs. controls)	Mean DVR	Hist. std	Hist. skewness	Hist. kurtosis	V_{50-90}
Pons	0.657	0.971	0.994	0.989	0.850
Cereb. peduncles	0.689	0.963	0.998	0.992	0.887
Putamen	0.637	0.972	1.00	0.999	0.995
Caudate	-	0.958	0.996	0.992	0.599
Parietal Cx	0.712	0.999	0.981	0.915	0.984

Table II: AUC values (SLE vs. controls)	Mean DV	NGTD Contrast
Pons	0.857	0.966
Midbrain	0.852	0.990
Cereb. peduncles	0.780	0.966
Thalamus	0.837	0.943
Hippocampus	0.821	0.910
Frontal Cx	0.859	0.993
Post-cingul. Cx	0.741	0.829

Fig. 1 provides a clear depiction of the improved separation between SLE patients vs. controls (frontal cortex) using the alternative formulation, as opposed to mean DV analysis.

Notably for SLE studies, as shown in **Table III**, our 3D-MI analysis also revealed quantitative J_1, J_2, J_3, and Q shape between the same ROIs as initially shown Table II. In fact, even when the PET values were set to unity within the ROIs, significantly different metrics were obtained (not shown), revealing different anatomical shapes between the two groups. This finding has raised the interesting question of whether vascular disease in these patients has an anatomic impact, which is an example of how the proposed framework can impact research.

This finding also leads one to attribute, at least partially, the improved AUC performance in Table II to modified/increased PVE; in such a scenario, PVE actually aids the discrimination capability (particularly using the NGTD contrast feature, which emphasizes both local heterogeneity and global range of uptake values) as it leads to increases apparent heterogeneity. Analogous observations of improved FDG PET tumor response classification in the presence of PVE have also been made [23, 24]. This issue has implications in terms of segmentation tasks, which need to be investigated, as to how inclusive they ought to be of edge voxels.

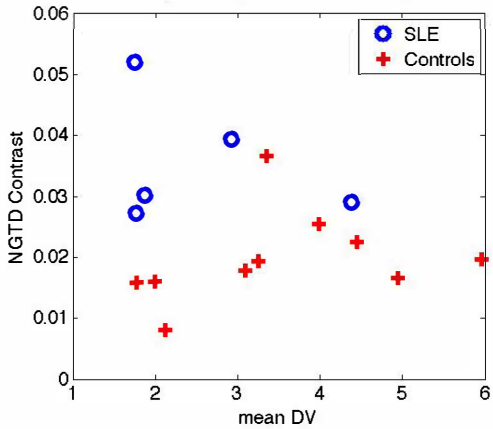

Figure 1. Plots of proposed heterogeneity measure (NGTD contrast) vs. conventional mean DV for the frontal Cx. Clear separation of the SLE population from controls is achieved in the proposed quantification approach, in contrast to conventional mean measure.

Table III: AUC values (SLE vs. controls)	Q	J1	J2	J3
Pons	0.984	0.988	0.983	0.967
Midbrain	0.983	0.982	0.976	0.967
Cereb. peduncles	0.890	0.954	0.997	0.997
Thalamus	0.947	0.966	0.959	0.868
Hippocampus	0.954	0.989	0.995	0.817
Frontal Cx	0.575	0.711	0.952	0.982
Post-cingul. Cx	0.865	0.848	0.822	0.772

Another consideration is the need for appropriate statistical analysis. This is because multiple metrics are applied to multiple ROIs, and statistical methods (e.g. Bonferroni-like) ought to be applied to properly assess the significance of positive findings. This observation is also true for tumor heterogeneity quantification approaches in the literature [3], wherein appropriate analysis remain to be developed.

Our framework requires elaborate ROI delineations, and as more images are gathered and more ROIs are drawn, the results and interpretations can be further refined.

IV. Conclusions

In this work, we have proposed a comprehensive framework to perform shape and texture analysis in parametric PET imaging. The approach provides a complementary tool to kinetic analysis, and has the potential to bring about a new quantification paradigm, for parametric imaging studies involving radiopharmaceutical hypothesized
to exhibit increased heterogeneity and/or shape changes with disease. The framework has the potential for: (i) enhanced discrimination, providing tools for additional analysis in research, and (ii) for use in diagnosis, staging & treatment.

Acknowledgment

The authors wish to thank Andrew Crabb for computational support.

References

[1] A. Rahmim and H. Zaidi, "PET versus SPECT: strengths, limitations and challenges," *Nucl Med Commun,* vol. 29, pp. 193-207, Mar 2008.

[2] M. Bentourkia and H. Zaidi, "Tracer kinetic modeling in PET.," *PET Clinics,* vol. 2, pp. *267-277*, 2007.

[3] M. C. Asselin, *et al.*, "Quantifying heterogeneity in human tumours using MRI and PET," *European Journal of Cancer,* vol. 48, pp. 447-455, Mar 2012.

[4] J. F. Eary, *et al.*, "Spatial Heterogeneity in Sarcoma (18)F-FDG Uptake as a Predictor of Patient Outcome," *Journal of Nuclear Medicine,* vol. 49, pp. 1973-1979, Dec 2008.

[5] F. Tixier, *et al.*, "Intratumor Heterogeneity Characterized by Textural Features on Baseline (18)F-FDG PET Images Predicts Response to Concomitant Radiochemotherapy in Esophageal Cancer," *Journal of Nuclear Medicine,* vol. 52, pp. 369-378, Mar 1 2011.

[6] I. El Naqa, *et al.*, "Exploring feature-based approaches in PET images for predicting cancer treatment outcomes," *Pattern Recognition,* vol. 42, pp. 1162-1171, Jun 2009.

[7] J. Flusser, *et al.*, *Moments and moment invariants in pattern recognition.* West Sussex, UK: Wiley & Sons, Inc., 2009.

[8] B. Ng, *et al.*, "Spatial Characterization of fMRI Activation Maps Using Invariant 3-D Moment Descriptors," *IEEE Transactions on Medical Imaging,* vol. 28, pp. 261-268, Feb 2009.
[9] M. Gonzalez, *et al.*, "Novel spatial analysis method for PET data using 3D moment invariants: applications to Parkinson's disease," *J. Cereb. Blood Flow & Metab.,* vol. 32 (suppl. 1), p. P117, 2012.
[10] V. Sossi, *et al.*, "New insights into levodpoa induced dopamine release in Parkinson's disease," *J. Cereb. Blood Flow & Metab.,* vol. 32 (suppl. 1), p. P114, 2012.
[11] F. A. Sadjadi and E. L. Hall, "Three-Dimensional Moment Invariants," *IEEE Trans Pattern Anal Machine Intell,* vol. PAMI-2, pp. 127-136, 1980.
[12] T. H. Reiss, "Features Invariant to Linear Transformations in 2d and 3d," *11th Iapr International Conference on Pattern Recognition, Proceedings, Vol Iii,* pp. 493-496, 1992.
[13] R. M. Haralick, *et al.*, "Textural Features for Image Classification," *Ieee Transactions on Systems Man and Cybernetics,* vol. Smc3, pp. 610-621, 1973.
[14] R. W. Conners, *et al.*, "Segmentation of a High-Resolution Urban Scene Using Texture Operators," *Computer Vision Graphics and Image Processing,* vol. 25, pp. 273-310, 1984.
[15] R. W. Conners and C. A. Harlow, "Toward a Structural Textural Analyzer Based on Statistical-Methods," *Computer Graphics and Image Processing,* vol. 12, pp. 224-256, 1980.
[16] G. Oh, *et al.*, "Fast determination of textural periodicity using distance matching function," *Pattern Recognition Letters,* vol. 20, pp. 191-197, Feb 1999.
[17] J. Parkkinen, *et al.*, "Detecting Texture Periodicity from the Cooccurrence Matrix," *Pattern Recognition Letters,* vol. 11, pp. 43-50, Jan 1990.
[18] J. Cohen, "A Coefficient of Agreement for Nominal Scales," *Educational and Psychological Measurement,* vol. 20, pp. 37-46, 1960.
[19] J. S. Weszka, *et al.*, "A Comparative Study of Texture Measures for Terrain Classification," *Systems, Man and Cybernetics, IEEE Transactions on,* vol. SMC-6, pp. 269-285, 1976.
[20] M. Amadasun and R. King, "Textural Features Corresponding to Textural Properties," *Ieee Transactions on Systems Man and Cybernetics,* vol. 19, pp. 1264-1274, Sep-Oct 1989.
[21] C. J. Endres, *et al.*, "Initial Evaluation of (11)C-DPA-713, a Novel TSPO PET Ligand, in Humans," *Journal of Nuclear Medicine,* vol. 50, pp. 1276-1282, Aug 2009.
[22] H. H. Barrett and K. J. Myers, *Foundations of Image Science*. Hoboken, New Jersey: Wiley & Sons, Inc., 2004.
[23] J. Maisonobe, *et al.*, "Is partial volume correction useful for detecting tumor uptake changes in patient monitoring?," *J Nuc Med,* vol. 51, pp. 27-, May 1, 2010 2010.
[24] J.-A. Maisonobe, *et al.*, "What is the best index to characterize early tumor response in FDG PET?," *J Nuc Med,* vol. 52, pp. 49-, May 1, 2011 2011.